Expanded View Figures

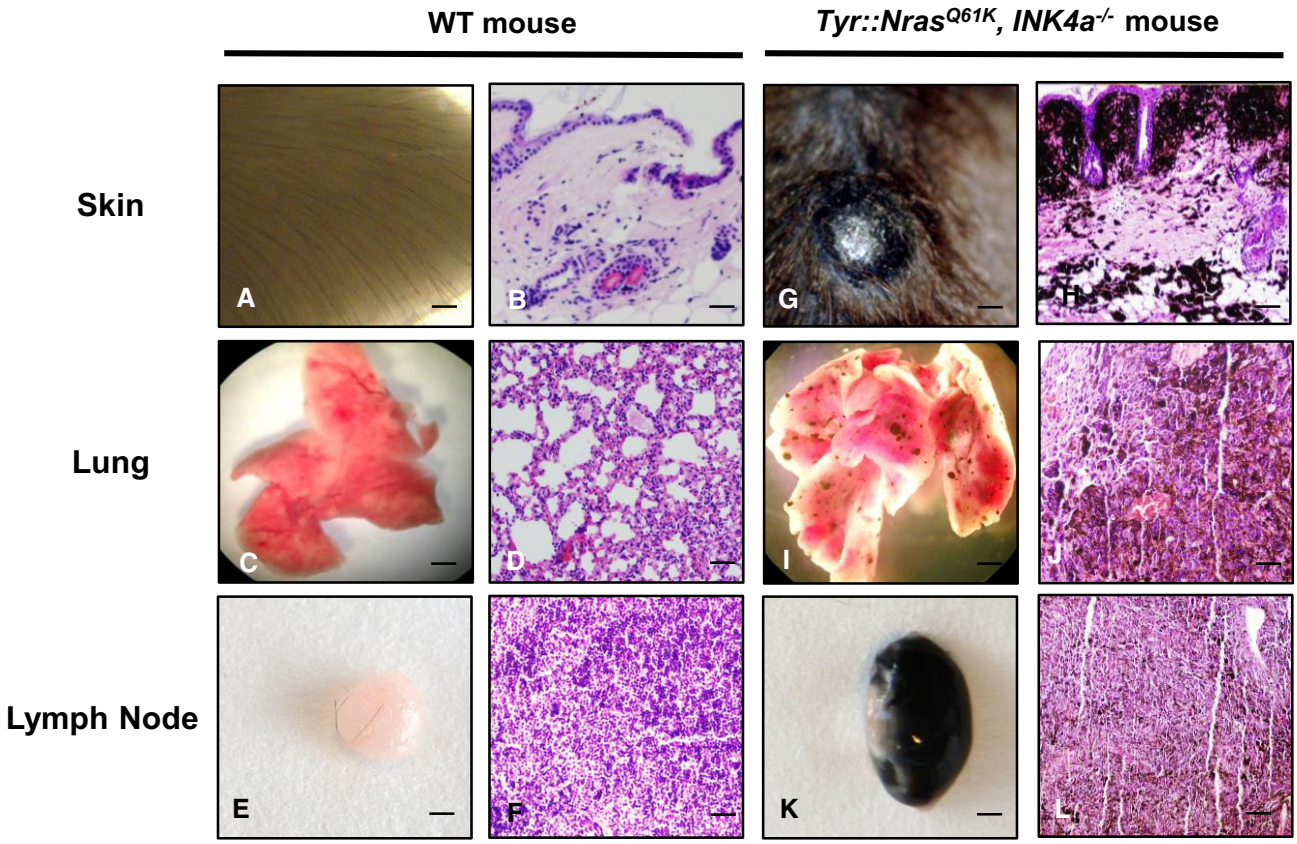

Figure EV1. *Tyr::Nras^{Q61K}INK4a$^{-/-}$* mouse model undergoes development of metastasis.

A–L Representative macroscopic pictures and H&E staining of sections taken from skin, lung, and lymph nodes (inguinal) of a metastatic melanoma bearing *Tyr::Nras^{Q61K}INK4a$^{-/-}$* mouse compared to an age-matched wild-type (WT) control animal. Picture panels: (A, C and E) represent wild-type (WT) skin, lung, and lymph node, respectively. (G, I and K) depict metastatic *Tyr::Nras^{Q61K}INK4a$^{-/-}$* skin, lung, and lymph node, correspondingly. H&E staining sections shown in panels (B, D, and F) represent WT skin, lung, and lymph node. Panels (H, J, and L) show metastatic *Tyr::Nras^{Q61K}INK4a$^{-/-}$* skin, lung, and lymph node, respectively. Scale bar for panels (A, C, E, G, I, and K) = 5 mm; scale bar for panels (B,D,F, H, J, and L) = 500 μm.

© 2018 The Authors

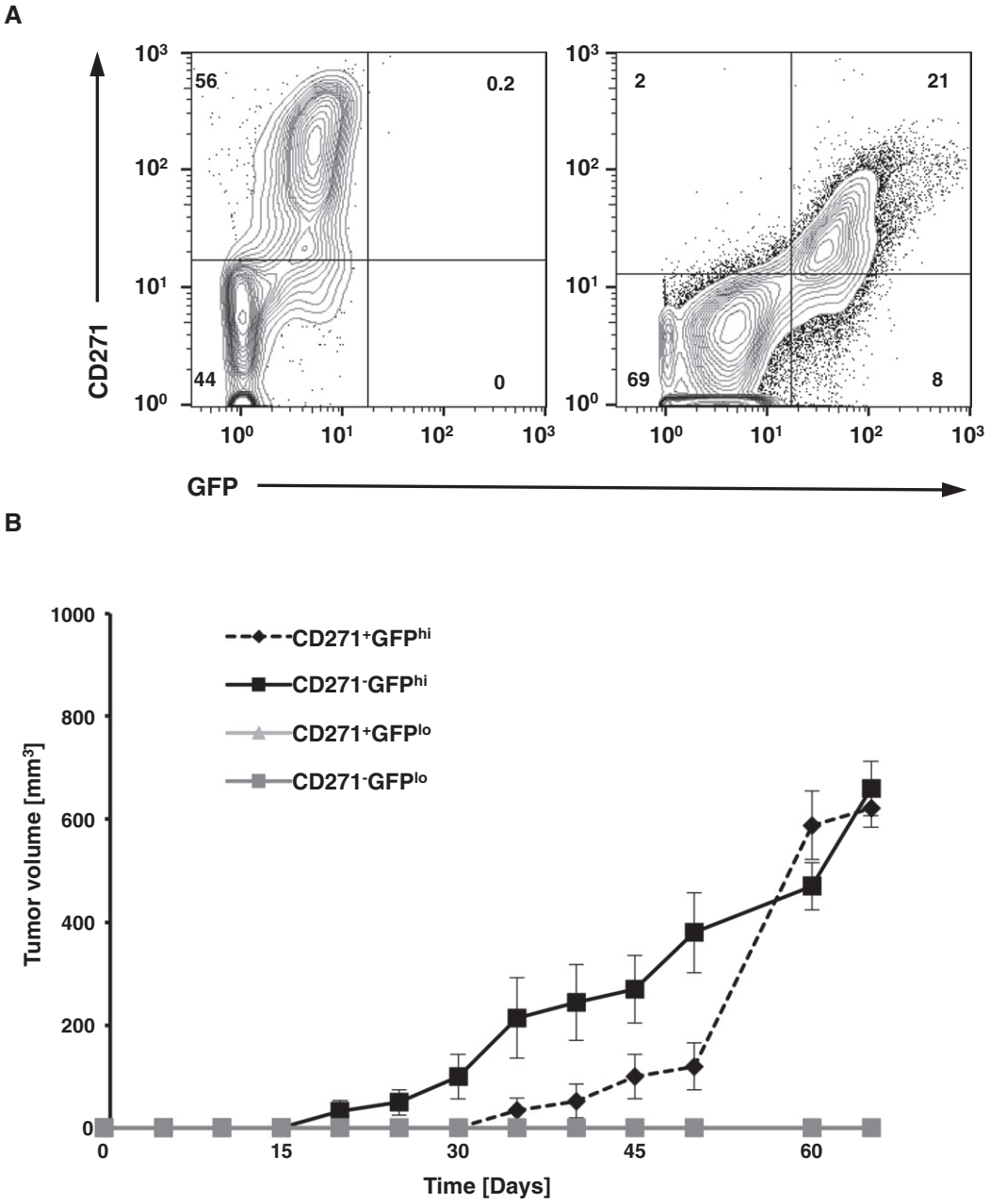

Figure EV2. Differential CD271 expression in *Tyr::Nras^{Q61K}INK4a$^{-/-}$*-driven melanoma does not alter tumor-initiating potential.

A Flow cytometric analysis shows representative FACS plots of GFP-c-Myc and CD271-expressing ($CD45^-CD31^-DAPI^-$) melanoma cells isolated from primary (skin) or metastic sites (LN) of a 7-month-old *Tyr::Nras^{Q61K}INK4a$^{-/-}$c-myc$^{G/G}$* animal.

B Graph shows tumor initiation and growth of sorted GFP-c-Myc^{hi} versus GFP-c-Myc^{lo} and/or CD271 (+) and (–) melanoma cells in Matrigel™ (1,000 s.c. cells per mouse) from *Tyr::Nras^{Q61K}INK4a$^{-/-}$c-myc$^{G/G}$* mice injected into Rag2$\gamma_c^{-/-}$ recipients. Groups were as follows: black filled diamond, $CD271^+GFP^{hi}$; black squares, $CD271^-GFP^{hi}$; gray triangles, $CD271^+GFP^{lo}$; gray squares, $CD271^-GFP^{lo}$ (n = 5 mice per group). For each time point, data are presented as mean ± standard deviation (s.d.).

 © 2018 The Authors

Figure EV3. JQ1-mediated downregulation of c-Myc in *Tyr::Nras^{Q61K}INK4a$^{-/-}$* melanoma cells interferes with cell growth and survival.

A, B Proliferation assay using alamarBlue® staining on *Tyr::Nras^{Q61K}INK4a$^{-/-}$c-Myc$^{+/+}$* mM1 melanoma cells (A) or mM1 melanoma cells stably transduced with a Cre-ERT construct (B) treated with either 4-OH-tamoxifen (4-OHT) to or ethanol (ETOH) as vehicle control. Data are presented as mean ± s.d. of one representative out of two independent experiments. In each experiment, all samples were done in triplicates.

C Proliferation analysis using alamarBlue® staining (left panel) and quantification of apoptosis by AnnexinV/7AAD staining (left panel) of *Tyr::Nras^{Q61K}INK4a$^{-/-}$c-Myc$^{+/+}$* mM1 cells treated with the bromodomain inhibitor (+)JQ1 to lower c-Myc expression levels. Inactive (−)JQ1 enantiomer was used as control. Data are presented as mean ± s.d. of one representative experiment. Two independent experiments were performed. In each experiment, all samples were done in triplicates. c-Myc protein levels were assessed by Western blot analysis.

D Quantification of apoptotic cells using AnnexinV/7AAD staining of B16F10 melanoma cells 48 or 72 h post siRNA-mediated knockdown of c-Myc (dark gray bars) versus control siRNA (light gray bars). Data are presented as mean ± s.d. of one representative out of two independent experiments. In each experiment, all samples were done in triplicates.

E Graph shows tumor growth of *Tyr::NRAS^{Q61K}INK4a$^{-/-}$c-Myc$^{+/+}$* (mM3) melanoma cells injected s.c. (1×10^5 mM3 cells per mouse) in Matrigel™ into Rag2$\gamma_c^{-/-}$ mice. At day 5 post-transplantation, animals with a tumor volume of 50 mm^3 were randomized into two groups (n = 6/group), injected with either (−)JQ1 (gray filled circles; 50 mg/kg/day) or (+)JQ1 (black filled circles; 50 mg/kg/day) starting on day 5. At experimental endpoint, tumors were harvested for gross morphology (bottom panel).

Data information: ***$P < 0.01$; Student's t-test.
Source data are available online for this figure.

© 2018 The Authors

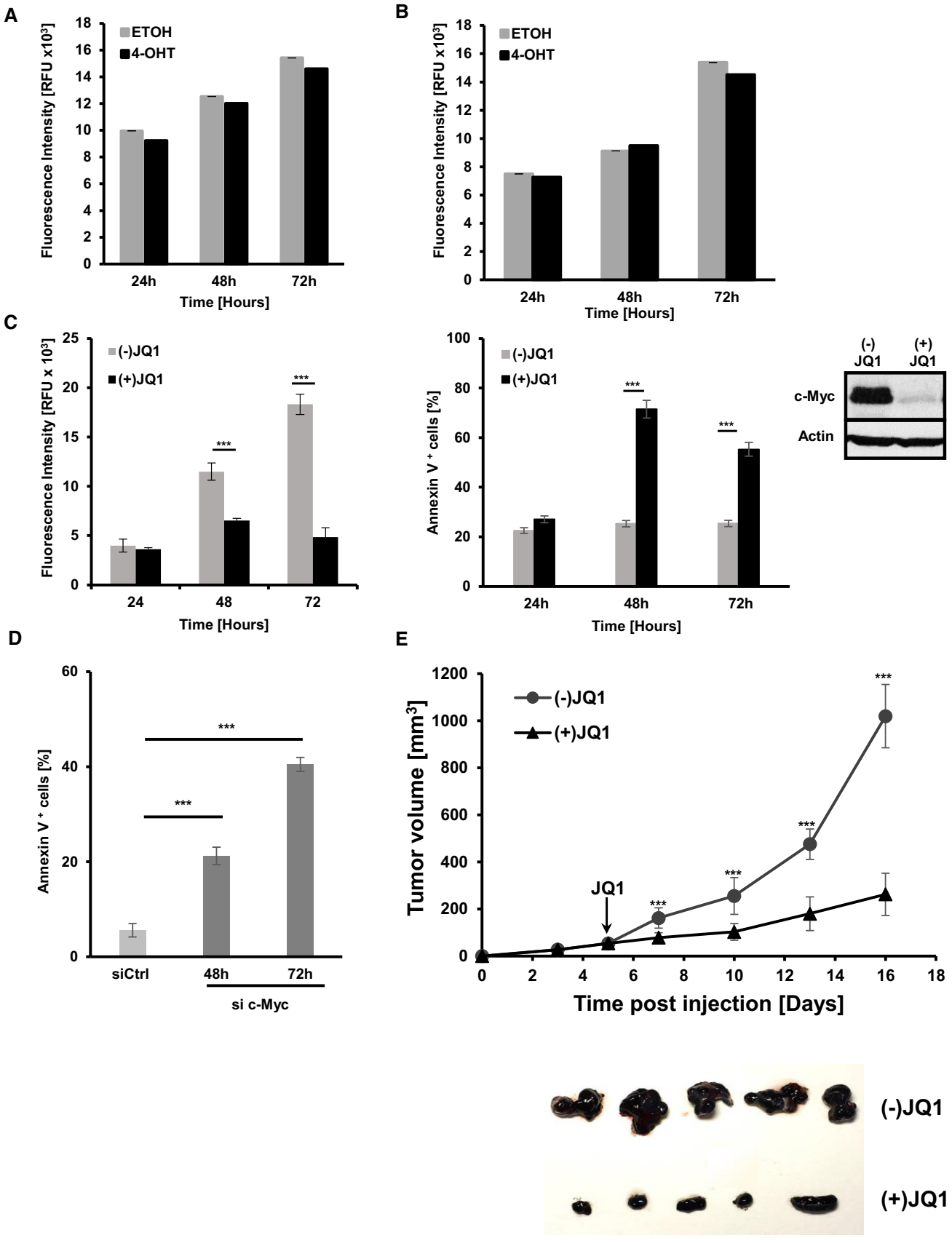

Figure EV3.

© 2018 The Authors

Figure EV4. siRNA-mediated downregulation of AMPK in mM1 and B16F10 melanoma cells induces cell death.

A Quantification of apoptotic cells using AnnexinV/7AAD staining of mM1 melanoma cells 48 or 72 h after treatment with either dorsomorphin (black bars) or vehicle control (light gray bars). Data are presented as mean ± s.d. of one representative out of two independent experiments. In each experiment, all samples were done in triplicates.

B, C Quantification of apoptotic cells using AnnexinV/7AAD staining of mM1 melanoma cells 48 or 72 h post siRNA-mediated knockdown of AMPKβ2 (B) or AMPKα1 (black bars, C) versus control siRNA (light gray bars). Data are presented as mean ± s.d. of one representative out of three independent experiments. In each experiment, all samples were done in triplicates. Knockdown efficiency of AMPKβ2 or AMPKα1 was confirmed by Western blot analysis at 48 and 72 h post-treatment.

D Quantification of apoptotic cells using AnnexinV/7AAD staining of B16F10 melanoma cells 48 or 72 h post siRNA-mediated knockdown of AMPKβ2 (*Prkab2*, dark gray bars) or AMPKα1 (*Prkaa1*, black bars) versus control siRNA (light gray bars). Data are presented as mean ± s.d. of one representative out of two independent experiments. In each experiment, all samples were done in triplicates. Knockdown efficiency of AMPKβ2 or AMPKα1 was confirmed by Western blot analysis 48 h post-treatment.

E Quantification of apoptotic cells by AnnexinV/7AAD staining of mM2 melanoma cells 24 and 48 h post Cre-ERT-mediated inactivation of c-Myc in the presence or absence of a constitutive active form of AMPKα (AMPKα CA). Ethanol (ETOH) and DMSO were used as vehicle controls. Data are presented as mean ± s.d. of one representative out of two independent experiments. In each experiment, all samples were done in triplicates.

F p-AMPK immunostaining was performed on representative sections from s.c. transplanted tumors excised either 5 or 9 days post initial JQ treatment [(−)JQ or (+)JQ at 50 mg/kg at day 7 post-transplantation]. Scale bars on images represent 200 μm.

Data information: ***$P < 0.01$, Student's *t*-test.
Source data are available online for this figure.

© 2018 The Authors

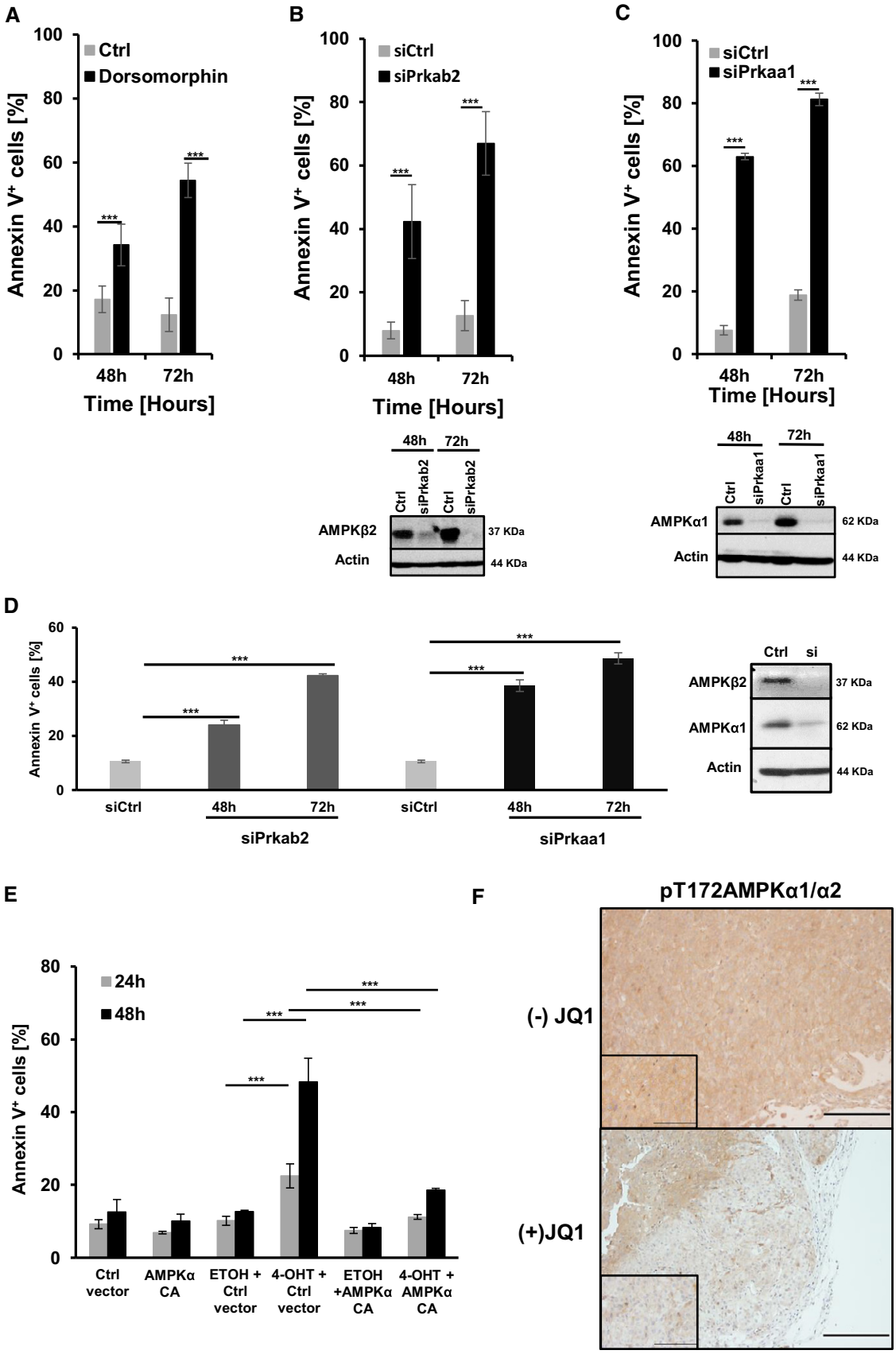

Figure EV4.

 © 2018 The Authors

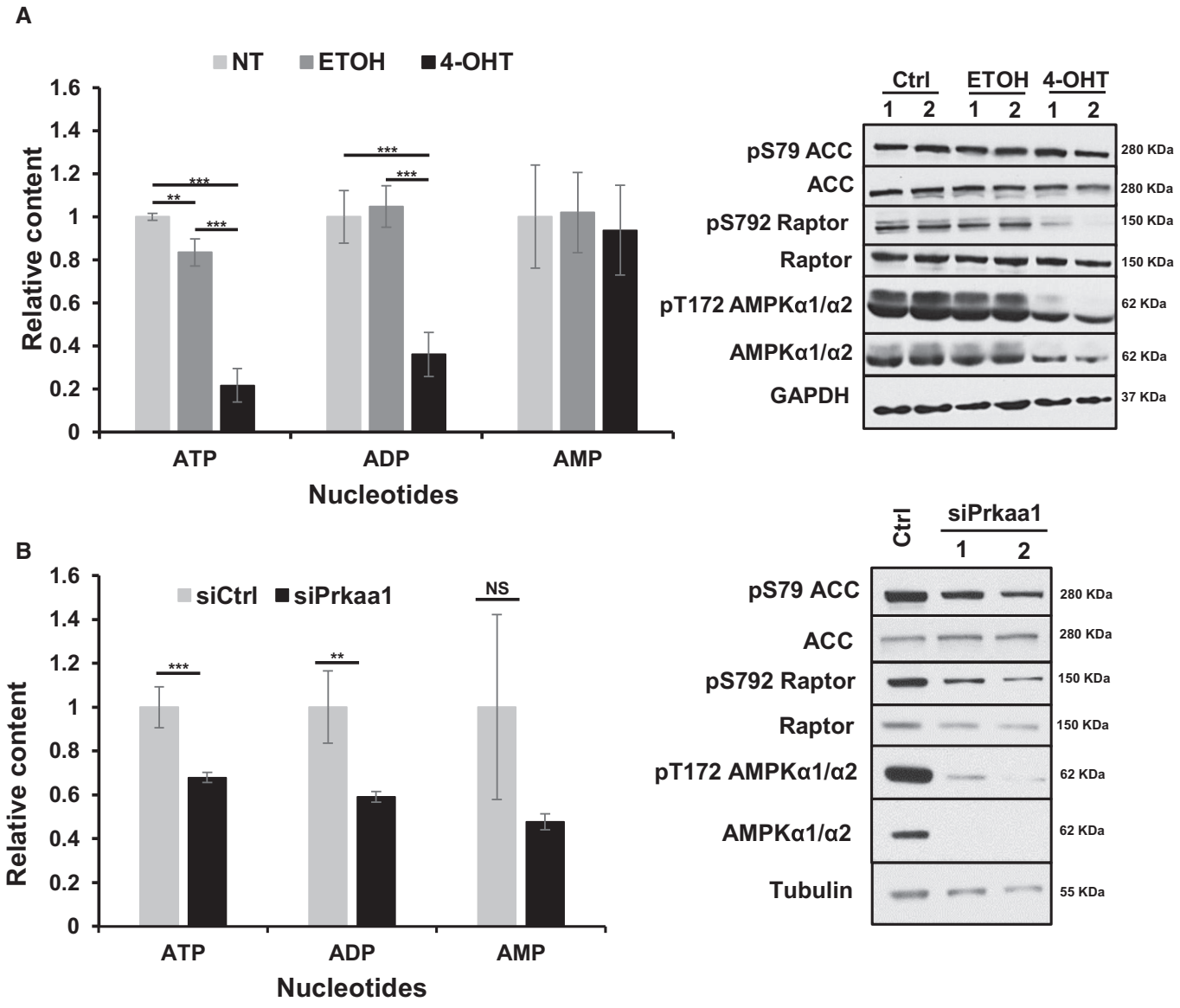

Figure EV5. c-Myc is a driving force for ATP production.

A Bar graph (left panel) depicts adenine nucleotide (ATP, ADP, and AMP) levels in mM2 cells either left untreated (Ctrl), treated with ethanol (ETOH) or genetic depletion of c-Myc (4-OHT) 48 h post-treatment, and normalized to total amino acid content. Right panel shows phosphorylation status of known AMPK targets in the mM2 mouse melanoma cell line in steady state and upon c-Myc inactivation 48 h post indicated treatments (untreated, Ctrl; vehicle, ETOH; c-Myc inactivation, 4-OHT).

B Bar graph (left panel) depicts ATP, ADP, and AMP nucleotide measurements in mM2 cells using siRNA-mediated knockdown of AMPKα1 (siPrkaa1, black bars) versus control siRNA (siCtrl, light gray bars) 48 h post-treatment and normalized to either protein content or total amino acid content. Right panel shows phosphorylation status of known AMPK targets in the mM2 mouse melanoma cell line in steady state and upon c-Myc inactivation 48 h post indicated treatments (control siRNA, siCtrl; AMPKα1 depletion, siPrkaa with two (1,2) independent siRNAs).

Data information: Data are presented as mean ± s.d. of one representative out of two independent experiments. In each experiment, all samples were done at least in triplicates. $^{**}P < 0.03$, $^{***}P < 0.01$, Student's *t*-test.
Source data are available online for this figure.

© 2018 The Authors